Giant Magnon-Polaron Anomalies in Spin Seebeck Effect in Double Umbrella-Structured $Tb_3Fe_5O_{12}$ Films

Yufei Li,[1,*] Yihang Duan,[2,3,*] Mingzhi Wang,[1] Lili Lang,[4] Yu Zhang,[1] Meng Yang,[5] Junxue Li,[5] Weijia Fan,[1] Ka Shen,[2,3,†] Zhong Shi,[1,‡] and Shi-Ming Zhou[1]

[1]*Shanghai Key Laboratory of Special Artificial Microstructure Materials and Technology and Pohl Institute of Solid State Physics and School of Physics Science and Engineering, Tongji University, Shanghai 200092, China*

[2]*Center for Advanced Quantum Studies and Department of Physics, Beijing Normal University, Beijing 100875, China*

[3]*Key Laboratory of Multi-scale Spin Physics, Ministry of Education, Beijing Normal University, Beijing 100875, China*

[4]*National Key Laboratory of Materials for Integrated Circuits, Shanghai Institute of Microsystem and Information Technology, Chinese Academy of Sciences, 865 Changning Road, Shanghai 200050, China*

[5]*Department of Physics, Southern University of Science and Technology, Shenzhen, Guangdong 518055, China*

(Received 23 August 2023; revised 24 October 2023; accepted 14 December 2023; published 31 January 2024)

We report a giant hysteretic spin Seebeck effect (SSE) anomaly with a sign reversal at magnetic fields much stronger than the coercive field in a (001)-oriented $Tb_3Fe_5O_{12}$ film. The high-field SSE enhancement reaches 4200% at approximately 105 K over its weak-field value and presents a nonmonotonic dependence on temperature. The unexpected high-field hysteresis of SSE is found to be associated with a magnetic transition of double-umbrella spin texture in TbIG. Nearly parallel dispersion curves of magnons and acoustic phonons around this neoteric transition are supported by theoretical calculations, leading to a high density of field-tuned magnon polarons and consequently an extraordinarily large SSE. Our study provides insight into the evolution of magnon dispersions of double-umbrella TbIG and could potentially boost the efficiency of magnon-polarons SSE devices.

DOI: 10.1103/PhysRevLett.132.056702

The spin Seebeck effect (SSE) in systems consisting of magnetic insulators and heavy metals has attracted significant attention since its discovery in 2010 [1,2], due to its unique potential for applications in spincaloritronic devices. In magnetic insulators, the spin current flows in the form of magnons and can be strongly affected by their interaction with phonons. An anomalous enhancement of SSE due to the hybridization of magnons and acoustic phonons was first observed in $Y_3Fe_5O_{12}$ (YIG)/Pt heterostructures in the pioneering work by Kikkawa *et al.* [3]. In the magnetic field dependence of SSE, the resonant-like anomalies were ascribed to the maximum density of magnon polarons (MPs), which are hybrid modes of magnons and phonons, occurring when their dispersions tangentially intersect [4–6].

To magnify the MP-induced SSE anomaly, one may consider promoting magnon-phonon hybridization at the tangent condition of the dispersions, for instance, by engineering the magnon/phonon dispersion or choosing magnetic materials with a larger magnetoelastic constant. A remarkable enhancement of the SSE anomaly was experimentally demonstrated in rare-earth iron garnets (ReIGs) $Lu_2BiFe_4GaO_{12}$ and $Gd_3Fe_5O_{12}$ (GdIG) [7–9], where the magnon dispersion was manipulated by atomic substitution and thermal effect, respectively.

Among the family of ReIGs, $Tb_3Fe_5O_{12}$ (TbIG) has a relatively strong anisotropy and a large magnetostriction constant due to the nonzero orbital angular momentum of Tb ions [10–13], which implies a potentially large MP-induced SSE anomaly in this material. Below the Néel temperature (T_N), the magnetic moments of Tb^{3+} ions arrange themselves into a collinear ferrimagnetic sublattice, antiparallel to the resultant iron magnetic moment, as predicted by the Néel's theory. However, at lower temperatures, a noncollinear arrangement of Tb^{3+} magnetic moments is observed, forming two conical structures with different cone angles, commonly known as the "double umbrella" magnetic structure [14,15]. The spin texture manifests itself a complicated evolution under a sweeping magnetic field and provides a unique opportunity to discover novel SSE properties, since the changes in magnetic structure may also affect the magnon dispersion. In this letter, we proposed a double-umbrella TbIG/Pt heterostructure and therein observed the giant magnon-polaron anomalies of SSE.

Figure 1(a) shows the schematic setup for the longitudinal SSE (LSSE) measurement of the TbIG/Pt heterostructure. An epitaxial 140-nm-thick TbIG film was deposited on a (001)-oriented $Gd_3Sc_2Ga_3O_{12}$ (GSGG) substrate by pulsed laser deposition (PLD). Another 5-nm-thick Pt film was sputtered on the top of TbIG by magnetron sputtering. The LSSE pattern is fabricated via 3D Lithography machine (TuoTuo Technology). An on-chip heater is fabricated to generate a vertical

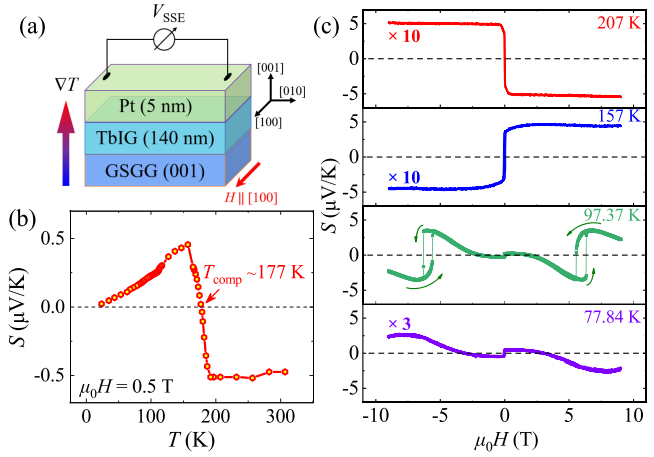

FIG. 1. (a) Device schematic for LSSE measurements in the GSGG(001)/TbIG(140 nm)/Pt(5 nm) sample. (b) Temperature dependence of the SSC at $\mu_0 H = 0.5$ T. (c) SSC as a function of magnetic field at typical temperatures.

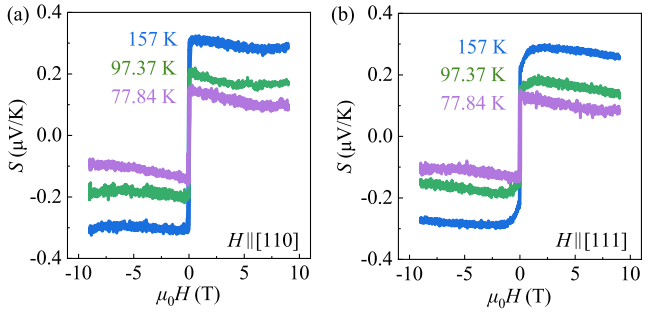

FIG. 2. The SSC as a function of the magnetic field along (a) [110] and (b) [111] directions, respectively.

temperature gradient ∇T. The open-circuit voltage was recorded as the SSE signal (V_{SSE}) when an in-plane magnetic field H is swept along the [100] axis. For quantitative characterization, the spin Seebeck coefficient (SSC) is derived from $S = [(V_{SSE}/\Delta T)/(L/d)]$, where d is the thickness of the GSGG substrate (much larger than that of the TbIG film), and L is the distance between two electrodes on the Pt layer. More details about the device fabrication and temperature gradient calibration are provided in Supplemental Material, Sec. I [16]. All electrical and thermal transport measurements were performed using a Physical Property Measurement System (PPMS).

The SSC as a function of temperature at 0.5 T is represented in Fig. 1(b). A sign change occurs at the compensation temperature ($T_{comp} \sim 177$ K), which is commonly demonstrated in ReIGs with magnetic rare-earth ions (Re^{3+}), such as GdIG [8,19–21]. The lower compensation temperature in our TbIG film, compared to the bulk value (~250 K), can be attributed to the effects induced by, for example, the inevitable defects, the strain from the substrate [20], etc. The decline of the SSC at low temperatures is due to the strong suppression of thermal magnon excitation [3]. In GdIG/Pt, a second sign change below T_{comp} was observed and attributed to the competition between magnon branches with opposite polarizations [8,9,19–21]. However, here in TbIG/Pt bilayer, the second sign change of SSC does not show up even down to 25 K. More interestingly, the magnetic field dependence of the SSC strongly relies on the temperature, as shown in Fig. 1(c). At 207 and 157 K, the SSC presents a common step-shaped sign change at the very small coercive field and saturates to nearly a constant in the high field range. Very interestingly, for the case of 97.37 K, the SSC shows an additional sign change around ±2 T, further followed by an unexpected hysteresis-like anomaly at approximately ±6 T. The SSC in this anomalous region is surprisingly magnified even by one order of magnitude with respect to the weak-field value. Such behaviors in TbIG/Pt are markedly distinct from previous observations in other magnetic-based heterostructures, where the SSC is typically suppressed by the magnetic field, and only minor MP-SSE anomalies have been reported [3–5,7–9,22–26]. With further decreasing temperature to 77.84 K, the hysteretic feature is no longer present, which is likely shifted outside the field range of the PPMS, while the low field (<5 T) sign change prevails.

These bizarre behaviors at 97.37 K inspired us to explore the SSE with different magnetic field orientations. Remarkably, as shown in Fig. 2, the hysteresis behavior completely vanishes in the same TbIG/Pt sample when the magnetic field H is applied along the [110] or [111] axis. Consequently, the significant enhancement of SSC is also absent, and the magnitude of the SSC is comparable to the weak-field value of the $H \parallel [100]$ case in Fig. 1(b).

To comprehend the physics behind these intriguing findings, we realize that the hysteresis-like feature holds the key to these mysteries. With the knowledge of hysteretic magnetization minor loops reported in the bulk TbIG crystal in comparable magnetic field range of our hysteresis-like SSC anomaly when the magnetic field is oriented along the [100] crystal axis [14,15], we speculate that the high-field SSE loop in current work might result from the same magnetic-structure transition. To confirm this conjecture, we carried out electrical measurements of longitudinal magnetoresistance (R_m) with the three magnetic field orientations (see Supplemental Material, Sec. III [16]). A jump of magnetoresistance is also observed only when the field is swept in the [100] direction, and the appearance of the magnetoresistance jump is found to be in the same temperature range and comparable magnetic fields of the SSE anomaly. Therefore, the high-field behaviors of SSC and R_m strongly suggest that there is an unconventional spin texture in TbIG, and consequently the magnetic-structure transition occurs at 97.37 K when the magnetic field is along the [100] direction. The discrepancy of the transition magnetic field in SSC and R_m might reflect the

distinct magnetic properties within the TbIG film and those at the interface.

Although several theoretical models have been proposed to interpret the origin of umbrella-type noncollinear magnetic configurations in ReIGs [27,28], to the best of our knowledge, characterization of the magnetic transition as a response to a magnetic field in TbIG remains beyond the scope of these models. Here, we extend the atomic exchange model based on a realistic garnet lattice geometry by taking into account an effective on-site anisotropy of Tb atoms to reproduce the zero-field double umbrella, and furthermore, to explain the observed magnetic transition at high magnetic fields (several teslas) around 97 K.

From the atomistic spin dynamics simulations based on the Landau-Lifshitz-Gilbert (LLG) equation [29,30]

$$\frac{d\boldsymbol{s}_i}{dt} = -\frac{\gamma}{1+\alpha_0^2}\boldsymbol{s}_i \times \boldsymbol{B}_i^{\text{eff}} - \frac{\gamma\alpha_0}{(1+\alpha_0^2)\sqrt{s_i(s_i+1)}}\boldsymbol{s}_i \times (\boldsymbol{s}_i \times \boldsymbol{B}_i^{\text{eff}}), \tag{1}$$

we obtain the evolution of the equilibrium magnetic configurations during the sweeping of the magnetic field along [100] direction. In Eq. (1), $\boldsymbol{s}_i$ is the spin magnetic moment for the i th atom, $\gamma = g\mu_B/\hbar$ is the gyromagnetic ratio and α_0 is the damping coefficient. The effective fields $\boldsymbol{B}_i^{\text{eff}}$ of $a(d)$-site Fe and c-site Tb sublattices can be expressed as

$$\boldsymbol{B}_{a_i(d_i)}^{\text{eff}} = \boldsymbol{B} + \frac{1}{g\mu_B}\left[J_{aa(dd)}\sum_j \boldsymbol{s}_{a_j(d_j)} + 2J_{ad}\sum_j \boldsymbol{s}_{d_j(a_j)} + 2J_{ac(dc)}\sum_{q=1}^{3}\sum_j \left(\boldsymbol{s}_{c_{q_j}} + \boldsymbol{s}_{c'_{q_j}}\right)\right], \tag{2}$$

$$\boldsymbol{B}_{c_{q_i}(c'_{q_i})}^{\text{eff}} = \boldsymbol{B} + \frac{2}{g\mu_B}\left[J_{ac}\sum_j \boldsymbol{s}_{a_j} + J_{dc}\sum_j \boldsymbol{s}_{d_j} + \sum_{\delta=1}^{2} K_{\delta,c(c')}\left(\boldsymbol{s}_{c_{q_i}(c'_{q_i})}\cdot \hat{k}_{\delta,c_q(c'_q)}\right)\hat{k}_{\delta,c_q(c'_q)}\right]. \tag{3}$$

More details of our theoretical model, including the site-dependent anisotropy axes $\hat{k}_{\delta,c_q(c'_q)}$ and the specific values of exchange and anisotropy coefficients are presented in Supplemental Material, Sec. IV [16].

The projection of the total magnetization in a primitive cell along the field direction is plotted as a function of the magnetic field strength in Fig. 3(a). As shown, our model successfully provides the magnetization loop in a magnetic field range comparable with the reported experimental results of the $M-H$ relation [14]. Figure 3(b) plots the magnetic field dependence of the orientation angle of the net Fe magnetization θ_{Fe} with respect to the $[\bar{1}00]$ axis (see inset), which clearly shows a sudden change at each jump. The simulated magnetic configurations at three typical cases for upsweeping are plotted in Figs. 3(c)–3(e), from which we find that the zero-field configuration reported in Ref. [14] is successfully reproduced by our model, and the high-field magnetization loop results from the transition of the c'_1 sublattice when its effective anisotropic magnetic field is overcome by the external field. Notably, our simulations with a sweeping magnetic field along the [110] or [111] directions do not show any magnetization jump (see Supplemental Material, Sec. IV [16]), which is also consistent with the observations in bulk TbIG [14,15]. Therefore, it is intuitive to expect that the umbrella-like magnetic sublattice and its aberrant high-field reorientation could play an essential role in the observed abrupt surge in SSC as the evolution of the magnetic structure also leads to a modification in spin dynamics and spin transport properties.

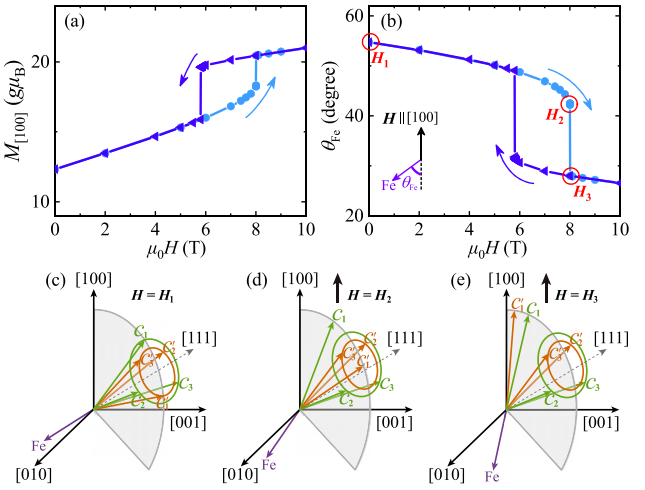

FIG. 3. (a) The simulated total magnetization M along the field direction [100] and (b) the orientation angle θ_{Fe} of the net magnetization from antiparallelly aligned a- and d-site Fe ions, as a function of the sweeping magnetic field in the [100] direction. (c) Schematic diagram of the zero-field ($\mu_0 H_1$) double umbrella magnetic structure. The magnetic moments of three Tb sublattices, c_1, c_2, and c_3 (c'_1, c'_2, and c'_3), form a cone magnetic structure in green (orange) around the [111] axis with 3-fold rotational symmetry. c_1 and c'_1 are located in the $(0\bar{1}1)$ plane. The net magnetic moment of Fe lies in the [111] direction. (d) and (e) are schematic diagrams of calculated magnetic configurations at $\mu_0 H_2 = 8.004$ and $\mu_0 H_3 = 8.006$ T for upsweeping, i.e., slightly before and after the magnetization jump at transition field, respectively.

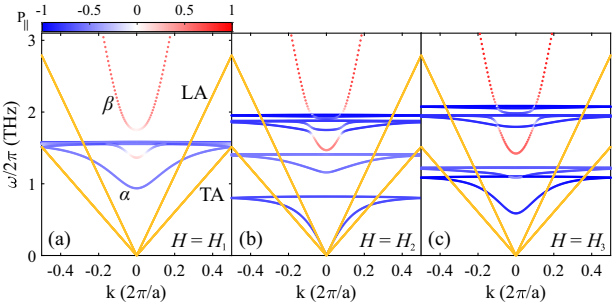

FIG. 4. The magnon spectra of bulk TbIG in the low-frequency regime (<3.1 THz) for the magnetic configurations at $H_1 - H_3$ in Fig. 3(b). The color scale of the magnon dispersion curves indicates the projection of the polarization along the magnetic field. The orange curves represent the dispersion curves of the longitudinal (LA) and transverse (TA) acoustic phonons with sound speeds $c_l = 6.08$ and $c_t = 3.3$ km/s [31], respectively.

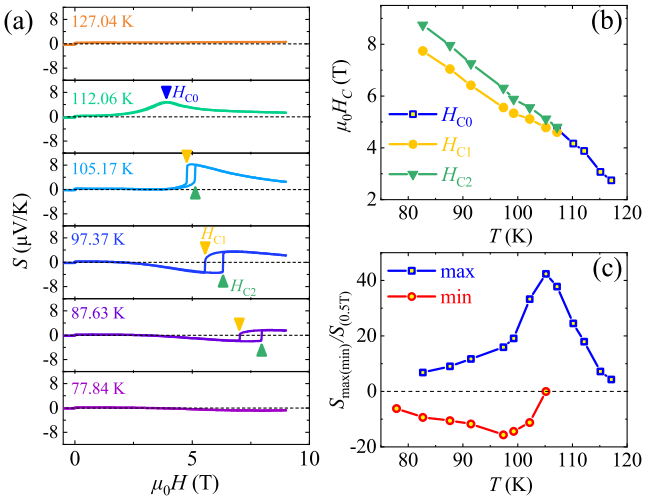

FIG. 5. (a) SSC as a function of magnetic field at different temperatures around the anomaly region. H_{C0} (indicated by blue arrow) is the position of the single precursory peak anomaly. H_{C1} and H_{C2} (indicated separately by yellow and green arrows) are the transition fields for down-sweeping and up-sweeping, respectively. The temperature dependence of (b) transition fields and (c) enhancement factor of the anomalies.

To explicitly analyze this effect, we extend the method in Ref. [9] to the noncollinear magnetic configuration and calculate the magnon spectra for the three configurations in Figs. 3(c)–3(e). The results in the low frequency regime are plotted in Fig. 4, where the color scale of the dispersion curves indicates the projection of the magnon spin polarization along the magnetic field direction and is evaluated from $P_{||} = \sum_i P_i \cos\varphi_i$. Here, P_i stands for the angular moment contributed from the i th spin, and φ_i is the angle between the equilibrium magnetic moment and the magnetic field direction (see Supplemental Material, Sec. IV [16]). The zero-field magnon spectrum in Fig. 4(a) looks very similar to that in GdIG [9], except for a larger magnon gap of the lowest (α) branch due to the strong anisotropy of the Tb atoms and anti-crossing features between the Fe-dominated β branch and those flat dispersionless branches dominated by the Tb sublattices. The latter originates from the noncollinear magnetic configuration. The large gap of the α branch suppresses the thermal excitation of this magnon branch and hence restrains its contribution to the SSE compared to GdIG, which may be the reason for the absence of the second sign change in the temperature dependence of the SSE signal below T_{comp} in the present case mentioned above.

As the external magnetic field increases, the magnon gap is reduced and finally vanishes at the transition magnetic field, as shown in Fig. 4(b). Because the magnon population obeys Bose-Einstein statistics, the SSE contribution from the α branch is enhanced significantly and dominates over the contribution from the β branch with opposite polarization, explaining the low-field (~2 T) sign change at 97.37 K in Fig. 1(c). More interestingly, the dispersion of the α branch in Fig. 4(b) becomes nearly parallel to the LA phonon dispersion, illustrated by the orange curves, in a quite wide momentum space in the low-frequency range. This suggests that the formation of a large number of MP states could also benefit the large enhancement of the SSE signal when the magnetic field approaches to the critical value H_2. In addition, the strong magnon-phonon coupling due to the large magnetoelastic coefficient in TbIG could also enlarge the degree of hybridization between phonon and α-magnon states with a relatively large frequency difference and hence contribute to the enhancement of the SSE anomaly around H_2. After the magnetic transition, as shown in Fig. 4(c), the α branch experiences a drastic uplift, leading to a remarkable reduction in its contribution to SSE and hence a sharp jump anomaly. The complicated hybridization features in these magnon spectra make the direct calculation of SSC rather difficult. Even though, an estimation based on a simplified magnon spectrum does support the key features of this qualitative analysis (see the Supplemental Material, Sec. V [16]). The larger magnitude observed after the jump, compared to the low field SSC, may be related to the rotation of Fe spins, which enlarges the spin projection of the β magnons, reflected by the color scale in Figs. 4(a) and 4(c). Other contributions to this enhancement might be the magnon polarons due to the hybridization of the β magnons and LA phonons or the size effect in our sub-micron film which are beyond the scope of our present theoretical model of bulk TbIG.

To explore more explicitly the stimulation and the evolution of the anomaly, we conduct meticulous magnetic-field dependent measurements at various temperatures around 97 K and plot a series of typical results in Fig. 5(a), where the loop clearly moves to higher magnetic fields as the temperature decreases [see also the temperature dependence of the transition fields in Fig. 5(b)]. In the meantime, the difference between the transition field for

down-sweeping (H_{C1}) and up-sweeping (H_{C2}) becomes larger. This might be attributed to the larger anisotropy field of the Tb sublattice, deduced from the larger opening angle of the umbrella texture at lower temperature [32]. It is worth noting that, a single precursory peak (H_{C0}) is observed at the temperatures above the formation of the anomaly loop, where the sublattice spins only experience a smooth change, instead of a sudden transition, during the field sweeping [see the results at 112.06 K in Fig. 5(a)]. As discussed in Supplemental Material, Sec. IV [16], the absence of the loop at higher temperature is also related to the closing umbrella structure.

For a quantitative characterization of the SSE enhancement at the anomaly, we plot in Fig. 5(c) the temperature dependence of the maximal positive (negative) enhancement factor, i.e., the ratio of the maximum (minimum) value for each SSC curve to S at $\mu_0 H = 0.5$ T at the same temperature, which shows a nonmonotonic behavior. The positive enhancement factor increases with decreasing temperature and reaches a maximum of 42 at ~105 K while the magnitude of the negative enhancement factor is found to reach a maximal value of 15 around 97 K. Results with more temperatures are provided in Supplemental Material, Sec. VI [16].

In summary, we have observed rich anomalous features in the magnetic field dependence of SSE measurements in TbIG/Pt below the compensation temperature, which are attributed to the field-induced transition of the noncollinear spin texture and the evolution of the magnon spectrum in TbIG supported by theoretical modeling with sublattice-dependent anisotropy of Tb ions. The position and shape of the anomalies display a pronounced sensitivity and dependence on temperature. The SSC is found to be remarkably enhanced around the anomaly, with a maximal enhancement factor of 42, which is much larger than reported values in other magnetic insulators. The reorientation of the Fe spins, the suppression of the magnon gap and the formation of magnon polarons around the magnetic transition are all proposed to contribute to the observed giant SSE anomaly. Our study demonstrates the potential to facilitate more efficient thermal spin transport devices by using the transition of noncollinear spin textures.

This work was financially supported by National Key Research and Development Program of China (Grant No. 2022YFA1204002), National Natural Science Foundation of China (Grants No. 11974047, No. 12374100, No. 12074285, No. 12374118, No. 11774259, No. 52271188, and No. 12274323), the Shanghai Municipal Science and Technology Major Project (2021SHZDZX0100), the Fundamental Research Funds for the Central Universities, Natural Science Foundation of Shanghai (Grant No. 23ZR1466800), Shanghai Sailing Program (22YF1456400), Guangdong Innovative and Entrepreneurial Research Team Program (Grant No. 2021ZT09C296), and Fundamental Research Fund No. 20220814162144001.

*These authors contributed equally to this work.
†Corresponding author: kashen@bnu.edu.cn
‡Corresponding author: shizhong@tongji.edu.cn

[1] K. Uchida, H. Adachi, T. An, T. Ota, M. Toda, B. Hillebrands, S. Maekawa, and E. Saitoh, Long-range spin Seebeck effect and acoustic spin pumping, Nat. Mater. **10**, 737 (2011).
[2] K. Uchida, H. Adachi, T. Ota, H. Nakayama, S. Maekawa, and E. Saitoh, Observation of longitudinal spin-Seebeck effect in magnetic insulators, Appl. Phys. Lett. **97**, 172505 (2010).
[3] T. Kikkawa, K. Shen, B. Flebus, R. A. Duine, K. Uchida, Z. Qiu, G. E. Bauer, and E. Saitoh, Magnon polarons in the spin Seebeck effect, Phys. Rev. Lett. **117**, 207203 (2016).
[4] B. Flebus, K. Shen, T. Kikkawa, K. Uchida, Z. Qiu, E. Saitoh, R. A. Duine, and G. E. W. Bauer, Magnon-polaron transport in magnetic insulators, Phys. Rev. B **95**, 144420 (2017).
[5] L. J. Cornelissen, K. Oyanagi, T. Kikkawa, Z. Qiu, T. Kuschel, G. E. W. Bauer, B. J. van Wees, and E. Saitoh, Nonlocal magnon-polaron transport in yttrium iron garnet, Phys. Rev. B **96**, 104441 (2017).
[6] R. Schmidt and P. W. Brouwer, Theory of the low-temperature longitudinal spin Seebeck effect, Phys. Rev. B **103**, 014412 (2021).
[7] R. Ramos, T. Hioki, Y. Hashimoto, T. Kikkawa, P. Frey, A. J. E. Kreil, V. I. Vasyuchka, A. A. Serga, B. Hillebrands, and E. Saitoh, Room temperature and low-field resonant enhancement of spin Seebeck effect in partially compensated magnets, Nat. Commun. **10**, 5162 (2019).
[8] B. Yang, S. Y. Xia, H. Zhao, G. Liu, J. Du, K. Shen, Z. Qiu, and D. Wu, Revealing thermally driven distortion of magnon dispersion by spin Seebeck effect in $Gd_3Fe_5O_{12}$, Phys. Rev. B **103**, 054411 (2021).
[9] K. Shen, Temperature-switched anomaly in the spin Seebeck effect in $Gd_3Fe_5O_{12}$, Phys. Rev. B **99**, 024417 (2019).
[10] M. Kubota, A. Tsukazaki, F. Kagawa, K. Shibuya, Y. Tokunaga, M. Kawasaki, and Y. Tokura, Stress-induced perpendicular magnetization in epitaxial iron garnet thin films, Appl. Phys. Express **5**, 103002 (2012).
[11] N. Kumar, N. G. Kim, Y. A. Park, N. Hur, J. H. Jung, K. J. Han, and K. J. Yee, Epitaxial growth of terbium iron garnet thin films with out-of-plane axis of magnetization, Thin Solid Films **516**, 7753 (2008).
[12] V. H. Ortiz, M. Aldosary, J. Li, Y. Xu, M. I. Lohmann, P. Sellappan, Y. Kodera, J. E. Garay, and J. Shi, Systematic control of strain-induced perpendicular magnetic anisotropy in epitaxial europium and terbium iron garnet thin films, APL Mater. **6**, 121113 (2018).
[13] E. R. Rosenberg, L. Beran, C. O. Avci, C. Zeledon, B. Song, C. Gonzalez-Fuentes, J. Mendil, P. Gambardella, M. Veis,

C. Garcia, G. S. D. Beach, and C. A. Ross, Magnetism and spin transport in rare-earth-rich epitaxial terbium and europium iron garnet films, Phys. Rev. Mater. **2**, 094405 (2018).
[14] M. Lahoubi, M. Guillot, A. Marchand, F. Tcheou, and E. Roudault, Double umbrella structure in terbium iron garnet, IEEE Trans. Magn. **MAG-20**, 1518 (1984).
[15] M. Lahoubi, Symmetry analysis of the magnetic structures in TbIG and Tb:YIG at low temperature, J. Phys. Conf. Ser. **340**, 012068 (2012).
[16] See Supplemental Material at http://link.aps.org/supplemental/10.1103/PhysRevLett.132.056702 for the main text, including details of sample preparation, characterization of microstructures, electrical measurement, LSSE measurement of samples with different temperatures, and theoretical model of double umbrella state, which includes Refs. [17–18].
[17] A. B. Harris, Spin-wave spectra of yttrium and gadolinium iron garnet, Phys. Rev. **132**, 2398 (1963).
[18] K. Shen, Finite temperature magnon spectra in yttrium iron garnet from a mean field approach in a tight-binding model, New J. Phys. **20**, 043025 (2018).
[19] S. Geprägs *et al.*, Origin of the spin Seebeck effect in compensated ferrimagnets, Nat. Commun. **7**, 10452 (2016).
[20] J. Cramer, E. J. Guo, S. Geprägs, A. Kehlberger, Y. P. Ivanov, K. Ganzhorn, F. Della Coletta, M. Althammer, H. Huebl, R. Gross, J. Kosel, M. Kläui, and S. T. B. Goennenwein, Magnon mode selective spin transport in compensated ferrimagnets, Nano Lett. **17**, 3334 (2017).
[21] Y. Li, D. Zheng, B. Fang, C. Liu, C. Zhang, A. Chen, Y. Ma, K. Shen, H. Liu, A. Manchon, and X. Zhang, Unconventional spin pumping and magnetic damping in an insulating compensated ferrimagnet, Adv. Mater. **34**, e2200019 (2022).
[22] Z. Shi, Q. Xi, J. Li, Y. Li, M. Aldosary, Y. Xu, J. Zhou, S. M. Zhou, and J. Shi, Role of magnon-magnon scattering in magnon polaron spin Seebeck effect, Phys. Rev. Lett. **127**, 277203 (2021).
[23] T. Kikkawa, K. Uchida, S. Daimon, Z. Qiu, Y. Shiomi, and E. Saitoh, Critical suppression of spin Seebeck effect by magnetic fields, Phys. Rev. B **92**, 064413 (2015).
[24] T. Kikkawa, K. Oyanagi, T. Hioki, M. Ishida, Z. Qiu, R. Ramos, Y. Hashimoto, and E. Saitoh, Composition-tunable magnon-polaron anomalies in spin Seebeck effects in epitaxial $Bi_xY_{3-x}Fe_5O_{12}$ films, Phys. Rev. Mater. **6**, 104402 (2022).
[25] W. Xing, Y. Ma, Y. Yao, R. Cai, Y. Ji, R. Xiong, K. Shen, and W. Han, Facet-dependent magnon-polarons in epitaxial ferrimagnetic Fe_3O_4 thin films, Phys. Rev. B **102**, 184416 (2020).
[26] J. Li, H. T. Simensen, D. Reitz, Q. Sun, W. Yuan, C. Li, Y. Tserkovnyak, A. Brataas, and J. Shi, Observation of magnon polarons in a uniaxial antiferromagnetic insulator, Phys. Rev. Lett. **125**, 217201 (2020).
[27] F. Tcheou, E. F. Bertaut, and H. Fuess, II—Neutron diffraction study of some rare earth iron garnets $R\mathrm{IG}(R = \mathrm{Dy}, \mathrm{Er}, \mathrm{Yb}, \mathrm{Tm})$ at low temperatures, Solid State Commun. **8**, 1751 (1970).
[28] B. Tomasello, D. Mannix, S. Geprägs, and T. Ziman, Origin and dynamics of umbrella states in rare-earth iron garnets, Ann. Phys. (Amsterdam) **447**, 169117 (2022).
[29] L. D. Landau and L. M. Lifshitz, On the theory of the dispersion of magnetic permeability in ferromagnetic bodies, Phys. Z. Sowjetunion **8**, 153 (1935).
[30] T. L. Gilbert, Classics in magnetics A phenomenological theory of damping in ferromagnetic materials, IEEE Trans. Magn. **40**, 3443 (2004).
[31] L.-W. Wang, L.-S. Xie, P.-X. Xu, and K. Xia, First-principles study of magnon-phonon interactions in gadolinium iron garnet, Phys. Rev. B **101**, 165137 (2020).
[32] M. Lahoubi, Temperature evolution of the double umbrella magnetic structure in terbium iron garnet, *Neutron Diffraction*, edited by I. Khidirov (Intech Open, London, 2012), Chap. 10, pp. 203–230.